

# Optimization of Wavelet-Based De-noising in MRI

Karel BARTUSEK<sup>1</sup>, Jiri PRINOSIL<sup>2</sup>, Zdenek SMEKAL<sup>2</sup>

<sup>1</sup>Inst. of Scientific Instruments, Academy of Sciences of the Czech Rep., Kralovopolska 147, Brno, 612 00, Czech Rep.

<sup>2</sup>Faculty of Elect. Engineering and Communication, Brno Univ. of Technology, Purkynova 118, 612 00 Brno, Czech Rep.

bar@isibrno.cz, prinosil@feec.vutbr.cz, smekal@feec.vutbr.cz

**Abstract.** *In the paper, a method for MR image enhancement using the wavelet analysis is described. The wavelet analysis is concentrated on the influence of threshold level and mother wavelet choices on the resultant MR image. The influence is expressed by the measurement and mutual comparison of three MT image parameters: signal to noise ratio, image contrast, and linear slope edge approximation. Unlike most standard methods working exclusively with the MR image magnitude, in our case both the MR image magnitude and the MR image phase were used in the enhancement process. Some recommendations are mentioned in conclusion, such as how to use a combination of mother wavelets with threshold levels for various types of MR images.*

## Keywords

Wavelet transformation, filtering technique, magnetic resonance imaging.

## 1. Introduction

The time of MRI (Magnetic Resonance Imaging) is limited by patients' comfort, non-stabilities and artifacts of the tomography system, and physical limits during dynamical applications as heart imaging or functional MRI. At present, fast methods of magnetic resonance (EPI) are used, which allows significant reductions of investigation time. Retrieved images have a low-signal-to-noise ratio (SNR) and small contrast. In the MR imaging microscopy or for very thin slices of plants it is possible to use the time averaging of signal for SNR improvement, which has no effect on spatial resolution in the image. Extending the measurement time is acceptable for such objects. But this is not feasible in medicine and therefore a post-process image filtering (image de-noising) has to be used for SNR improvement. The drawback of each digital image filtering technique is the reduction of sharpness, resolution, and image contrast.

It is well known that magnitude image data of magnetic resonance obey the Rician distribution. Unlike additive Gaussian noise, Rician "noise" is signal-dependent, and separating signal from noise is a difficult task. Rician

noise is especially problematic in low signal-to-noise ratio (SNR) regimes where it not only causes random fluctuations, but also introduces a signal-dependent bias into the data that reduces image contrast.

The application of wavelets for the de-noising of MR images has been pioneered by Weaver et al. [1], who applied their de-noising scheme to MR images of the human neck. They concluded that the de-noising scheme can reduce noise by 10% to 50% without reducing edge sharpness.

De-noising techniques operating with magnitude images have been proposed in most cases only for disease diagnostic from MR images with a low signal-to-noise ratio. Henkelman [2] shows the relationship of the true signal amplitude to that which is measured in real and magnitude images in presence of noise. Correction factors for actual experimental measurements are demonstrated. Some recent work by Nowak [3] employs a wavelet-based method for de-noising the square magnitude images, and explicitly takes into account the Rician nature of the noise distribution.

A few works have been devoted to phase image de-noising, despite the existence of important applications like current density imaging (CDI), MRI and functional MRI. Alexander [4] applies a wavelet de-noising algorithm directly to the complex image obtained as the Fourier transform of the raw k-space two-channel (real and imaginary) data. By retaining the complex image, he is able to de-noise not only magnitude images but also phase images. A multi-scale (complex) wavelet-domain Wiener-type filter is derived. The algorithm preserves the edges when the Haar wavelet rather than smoother wavelets, such as those of Daubechies, are used. Zaroubi [5] presents a fast post-processing method for noise reduction of MR images, termed complex de-noising. The method is based on shrinking noisy discrete wavelet transform coefficients via thresholding, and it can be used for any MRI data-set with no need for high power computers. The de-noising algorithm is applied to the two orthogonal sets of complex MR images separately. Cruz-Enriquez [6] applies a group of de-noising algorithms in the wavelet domain to the complex image, in order to recover the phase information. Significant improvements in SNR for low initial values are achieved by using the proposed filters.

## 2. Materials and Methods

### 2.1 MRI Data

For real MRI data, a set of 2D phantom MR single-slice data from the same volunteer was acquired on a 4.7T MRI scanner (Magnex magnet, MR Solution electronic and software) in ISI Brno, using the standard spin-echo sequence. The sample applied was a square container (40x40x40 mm) filled with water. Relaxation times of water were reduced by the application of nickel sulphate. The cylindrical cuvette of 20mm diameter was filled with gel water sample, whose relaxation times are short (11 ms), and then inserted into a dish. The tested MR images with different SNR ( $T_E = 20$  ms,  $T_R = 500$  ms MA = 512x512, FOV = 60x60 mm) were coronal slices with the variable thickness (0.2 - 0.5 - 1 - 2 mm). In addition, the MR images of head (with TMJ) were acquired on the Philips ACHIEVA MRI system (DS = 1.5T) in the Faculty Hospital Brno-Bohunice. Measurement parameters were: T2W-FSE pulse sequence:  $T_E = 20$  ms,  $T_R = 1600$  ms, MA = 256x256, FOV = 160 x 160 mm, sagittal slice 2 mm.

### 2.2 SNR, Contrast and Slope Edge Estimates

For phantom MRI images with different SNR, the improvement of the SNR, contrast and linear slope edge approximation are measured before and after the application of de-noising algorithm. The SNR and contrast are computed in two regions of interest in each image: the first region contains only noisy background, while the second region contains, in addition, the signal. We use the definition of parameters according to (1) and (4). The linear slope edge approximation is estimated over a selected sharp edge in the MRI image.

The SNR in MR image is computed as the squared mean intensity of the selected area relative to the underlying Gaussian noise variance  $\sigma_N^2$ . The SNR of the image magnitude is defined as [3]

$$SNR = 10 \log_{10} \left( \frac{I_{\text{mean}}^2}{\sigma_N^2} \right) \quad (1)$$

where  $I_{\text{mean}}$  is obtained as the mean value of intensity  $I$  in a homogenous region-of-interest (ROI) inside the image (signal), and  $\sigma_N$  is the standard deviation of the ROI without signal (background). Considering the MR image averaging with the number of acquisitions  $N_{\text{acq}}$ , the standard deviation of noise is equal to

$$\sigma_{\text{eff}} = \frac{\sigma_N}{\sqrt{N_{\text{acq}}}}. \quad (2)$$

The contrast of image intensity  $I$  is defined as

$$C_{AB} = |I_A - I_B|. \quad (3)$$

The relative contrast is defined as the contrast which is related to reference image intensity  $I_{\text{ref}}$  ( $I_{\text{ref}} = (I_A + I_B)/2$ )

$$C_{\text{rel}} = \left( \frac{C_{AB}}{I_{\text{ref}}} \right) = 2 \cdot \frac{|I_A - I_B|}{I_A + I_B} \quad (4)$$

where  $I_A$  and  $I_B$  are the mean image intensities of A and B image areas, as shown in Fig. 1.

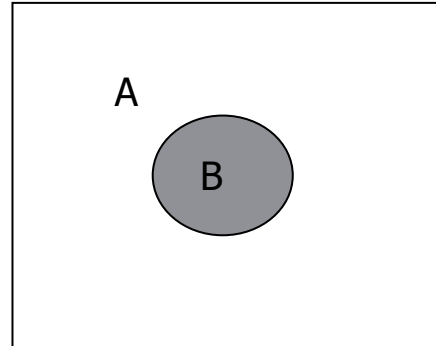


Fig. 1. MR image of the phantom for the contrast definition.

The linear slope edge approximation  $m$  can be estimated using (5) applied to a selected sharp edge, which is represented as 1D signal. Due to the presence of noise in the MR image, the measurement is realized on several places of the edge and the median of measurements is computed

$$m = \frac{\Delta y}{\Delta x} \quad (5)$$

where  $\Delta y$  and  $\Delta x$  represent the gradients of image intensity and scale, respectively, as shown in Fig. 2.

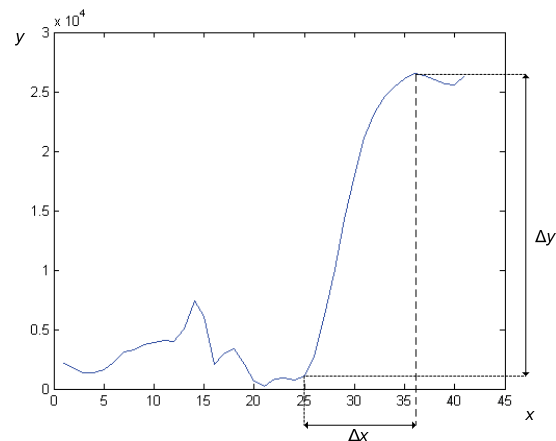


Fig. 2. An example of the linear slope edge estimation.

### 2.3 De-noising Algorithms

As already mentioned above, we utilize a wavelet-based algorithm for MR image noise reduction. The wavelet transform WT is an integral transform for the “time-frequency” description of analyzed signal. It can be used in various signal processing applications, e.g. signal compression, feature extraction, and noise removal. In our case, we use the two dimensional dyadic discrete-time wavelet transform 2D-DTWT, which uses mother wavelet function  $\varphi$  to decompose a digital image into a multilevel set of

approximations: vertical, horizontal and diagonal wavelet coefficients  $c'_{A}$ ,  $c'_{DV}$ ,  $c'_{DH}$ , and  $c'_{DD}$ , where  $l = 1, 2, \dots, L$  give the level of decomposition. A more detailed description of the wavelet transform and its properties can be found, for example, in [7]. The most frequently used technique for MR image noise reduction using the wavelet coefficients is thresholding. It is assumed that the wavelet coefficients with values lower than a particular threshold value  $T$  correspond to noisy samples and they can be therefore cancelled, which leads to noise reduction in the image domain. When the remaining coefficients are unaffected, it is called *hard* thresholding

$$\hat{c}(x, y) = \begin{cases} c(x, y) & |c(x, y)| \geq T \\ 0 & |c(x, y)| < T \end{cases} \quad (6)$$

Another often used kind of thresholding technique is the so-called *soft* thresholding, defined as

$$\hat{c}(x, y) = \begin{cases} \text{sign}[c(x, y)] \cdot [|c(x, y)| - T] & \text{for } |c(x, y)| \geq T \\ 0 & \text{for } |c(x, y)| < T \end{cases} \quad (7)$$

It can be generally said that soft thresholding yields a better SNR while hard thresholding better preserves the slope edge. There are other thresholding techniques such as semi-soft, hyperbolic, non negative garrote, etc. [8].

The most important part of the de-noising algorithm is the estimation of the optimal threshold value. When the threshold value is too low, then the noise reduction is inefficient, and, on the other hand, when it is too high, then details of image information can be lost. In our work, we consider one of the most frequently used estimation algorithms, the so-called *universal threshold*, defined as [10]

$$T = \sigma_{\text{est}} \cdot \sqrt{2 \cdot \log(N)} \quad (8)$$

where  $N$  is the number of input image pixels,  $\sigma_{\text{est}}$  represents the standard deviation of noise, which can be estimated by the Donoho and Johnstone theorem [9] as statistical median MAD of detailed wavelet coefficients  $c'_{DV}$ ,  $c'_{DH}$ , and  $c'_{DD}$  from the first decomposition level divided by the constant 0.6745 [9]. This threshold is then applied to all detailed wavelet coefficients of each decomposition level

$$\sigma_{\text{est}} = \frac{\text{MAD}(c'_D)}{0.6745} \quad (9)$$

When we consider de-noising a complex MR image, we have to first separate it into the real and imaginary parts. Then we process both parts by the wavelet transform separately, we estimate the unique threshold values for each part, and then threshold the wavelet coefficients. After that we reconstruct the image domain from the thresholded wavelet coefficients and, finally, combine them to form a de-noised complex image. The noise in both parts is assumed to be independent. The type of mother wavelets and thresholding techniques can differ for both parts.

In addition to the standard de-noising technique operating with thresholding, we also implement a method described in [4] with the Wiener filter applied to the complex wavelet coefficients (composed of the wavelet coefficients from the real and imaginary image parts). The method defined in (10) can be described as a multiplication of  $l$ -th decomposition level of detailed complex wavelet coefficients  $c^l(x, y)$  by the complex value of “attenuation” factor  $\alpha^l(x, y)$

$$\hat{c}^l(x, y) = \alpha^l(x, y) \cdot c^l(x, y). \quad (10)$$

According to [4], the attenuation factor for each wavelet coefficient can be evaluated using the magnitude value of the particular coefficient and the estimated standard deviation of noise  $\sigma_{\text{est}}$

$$\alpha^l(x, y) = \left[ \frac{|c^l(x, y)|^2 - \sigma_{\text{est}}^2}{|c^l(x, y)|^2} \right]_+ \quad (11)$$

Negative values of the attenuation factor are zeroed, i.e. coefficients with lower values than the estimated standard deviation of noise are eliminated, which can be computed as

$$\sigma_{\text{est}} = \sqrt{\sigma_{\text{est(R)}}^2 + \sigma_{\text{est(I)}}^2} \quad (12)$$

where  $\sigma_{\text{est(R)}}$  is the estimated standard deviation of noise from the real MR image part and  $\sigma_{\text{est(I)}}$  from the imaginary MR image part, using (9).

Equation (11) is extended by introducing an optional parameter  $\tau \geq 1$ , which allows the removal of the lower-value coefficients. Various values of  $\tau$  are suitable for different images [4]

$$\alpha^l(x, y) = \left[ \frac{|c^l(x, y)|^2 - \tau \cdot \sigma_{\text{est}}^2}{|c^l(x, y)|^2} \right]_+ \quad (13)$$

An advantage of this method is the combination of hard thresholding for high values of  $|c^l(x, y)|$  ( $\alpha^l(x, y) \approx 1$ ), which yields a small bias (better contrast and slope edge), and soft thresholding for coefficients with values close to the level of noise, which yields a small variance (better SNR).

## 3. Experiments and Results

### 3.1 Experiment Background

Our experiment can be divided into two parts. In the first part, the wavelet-based de-noising algorithms described above are applied to the phantom MRI, mentioned in section 2.1.

MR images with different signal-to-noise ratio (11.4 dB and 19.1 dB) for the verification of wavelet-based de-noising were obtained by measuring the transversal

sections of phantom for different thickness. The phantom consisted of deionized water, in which a cylinder filled with water and nickel sulfate was included (to reduce relaxation times and achieve the necessary image contrast) Fig. 1.

Several discrete mother wavelets (wavelet filters) are applied and the results are compared with the help of three described parameters (section 2.2). In the experiment, we use two images with different SNR (11.4 dB and 19.1 dB) obtained by varying the slice thickness. The contrast and the linear approximation of the slope edge are related to the reference image (ratio expression) with  $SNR = 35$  dB, because of unreliable measurement of these parameters from noisy images. In the second part of our experiment, the same procedure is performed on the MR image of head with  $SNR = 33$  dB, as mentioned in section 2.1.

The choice of mother wavelets has been inspired by a paper [11] dealing with analytical study of wavelet filters (mother wavelets) for image compression. The first change is the modification via replacing the Daubechies mother wavelet of the 7<sup>th</sup> order by the same mother wavelet of the 2<sup>nd</sup> order (more frequently used in MR de-noising) and by adding the discrete Meyer mother wavelet (often used in MR de-noising [12]). Another change consisted in applying the following mother wavelets: Haar, Daubechies 2<sup>nd</sup> and 9<sup>th</sup> orders, bi-orthogonal 2<sup>nd</sup>.2<sup>nd</sup> and 4<sup>th</sup>.4<sup>th</sup> orders, Symlet 5<sup>th</sup> order, Coiflet 5<sup>th</sup> order and discrete Meyer. According to experiments in paper [4], the level of the wavelet decomposition is 3. The complex image wavelet coefficient filtering is only considered, because filtering the coefficients of magnitude image wavelets introduces a signal-dependent bias, as shown in Fig. 3.

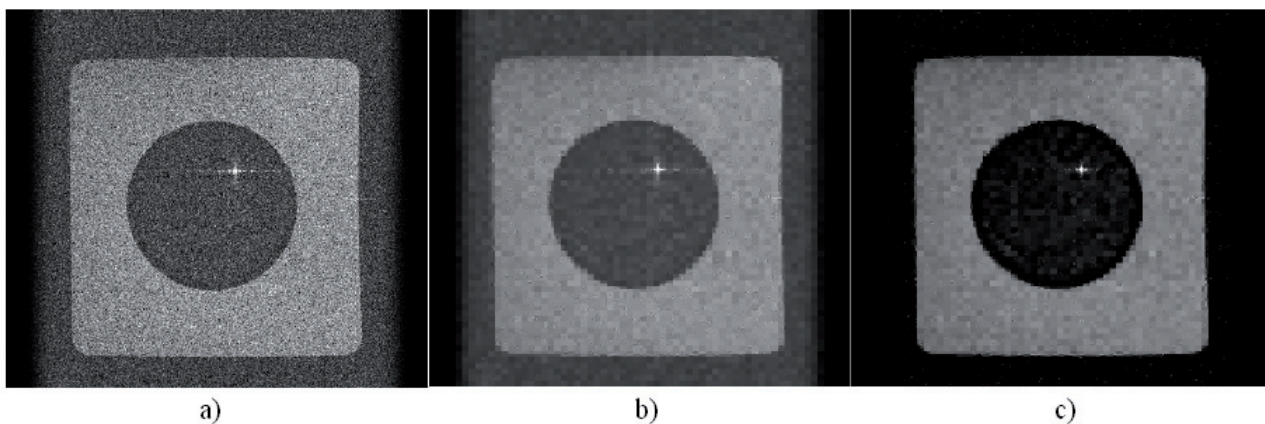


**Fig. 3.** a) The original MR image of the phantom having  $SNR = 11.4$  dB, b) magnitude image wavelet coefficients filtering with  $SNR=27$  dB, c) complex image wavelet coefficients filtering with  $SNR=25$  dB.

### 3.2 Results

Results of de-noising the phantom MR image with  $SNR = 11.4$  dB are shown in Tab. 1, and graphically in Fig. 4, where the values are normalized according to the reference value corresponding to the maximum value of a particular parameter.

The hard thresholding technique best preserves the slope edge for all wavelet filters, but it yields a lower SNR value in comparison with the soft thresholding technique.

Using the Wiener filtering technique, we reach the greatest balance between the values of SNR and slope edge for all wavelet types (except bior2.2) and, in addition, we also reach the best contrast. Generally, the contrast value should be the highest for a thresholding technique yielding the lowest bias, i.e. hard thresholding, but in the case of a low original MR image SNR the contrast is strongly affected by the presence of noise and therefore better results can be achieved even by a technique with higher bias, i.e. soft thresholding.

Wavelet filter	Hard thresholding			Soft thresholding			Wiener filtering		
	$SNR$	$C_{rel}$	$m$	$SNR$	$C_{rel}$	$m$	$SNR$	$C_{rel}$	$m$
haar	16.4	0.74	1.17	22.2	0.80	1.14	24.4	1.03	1.17
db2	16.3	0.75	0.50	21.3	0.81	0.41	24.6	1.02	0.52
db9	16.8	0.70	0.51	22.2	0.80	0.44	25.1	0.97	0.41
bior2.2	14.4	0.63	0.66	20.7	0.78	0.50	19.4	0.84	0.50
bior4.4	16.0	0.71	0.55	21.9	0.80	0.43	23.5	0.98	0.46
sym5	15.8	0.69	0.55	22.1	0.80	0.47	23.0	0.97	0.48
coif5	16.4	0.72	0.54	22.1	0.80	0.48	24.3	1.00	0.55
dmey	15.0	0.63	0.60	21.8	0.79	0.47	21.3	0.90	0.50

**Tab. 1.** Results of de-noising the phantom MR image with  $SNR = 11.4$  dB.

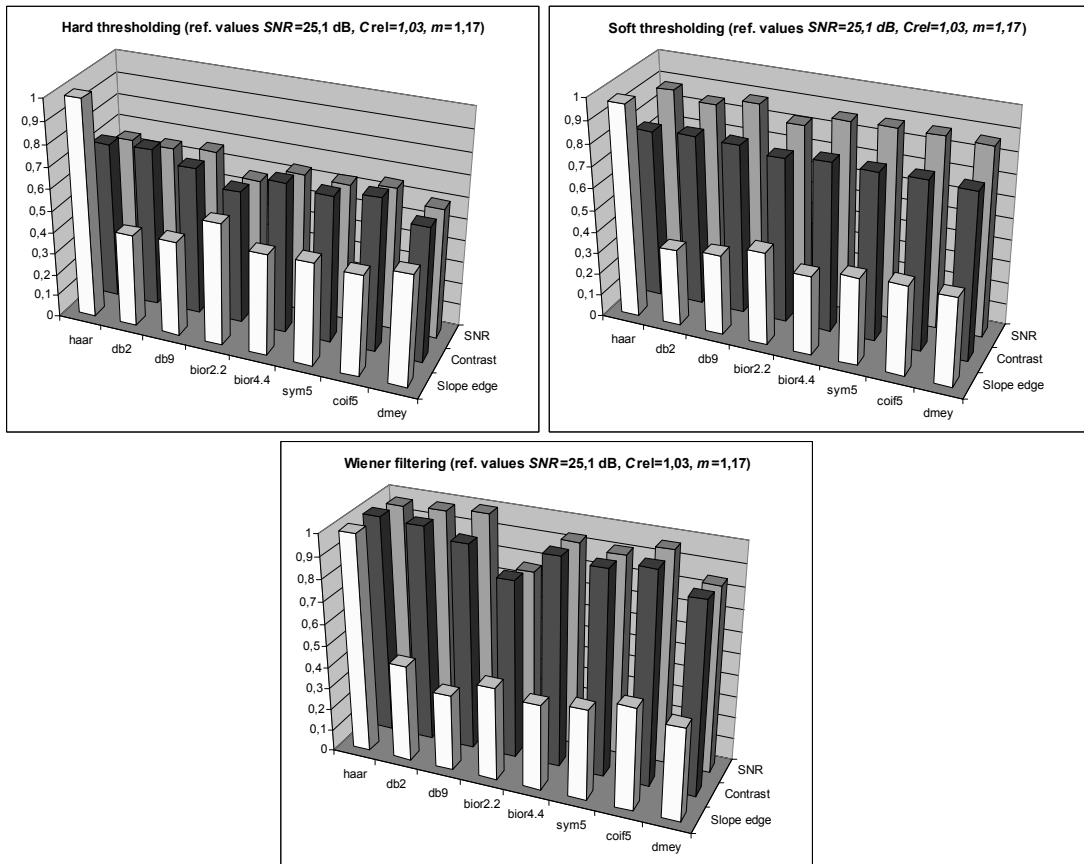


Fig. 4. Results of de-noising the phantom MR image with SNR = 11.4 dB.

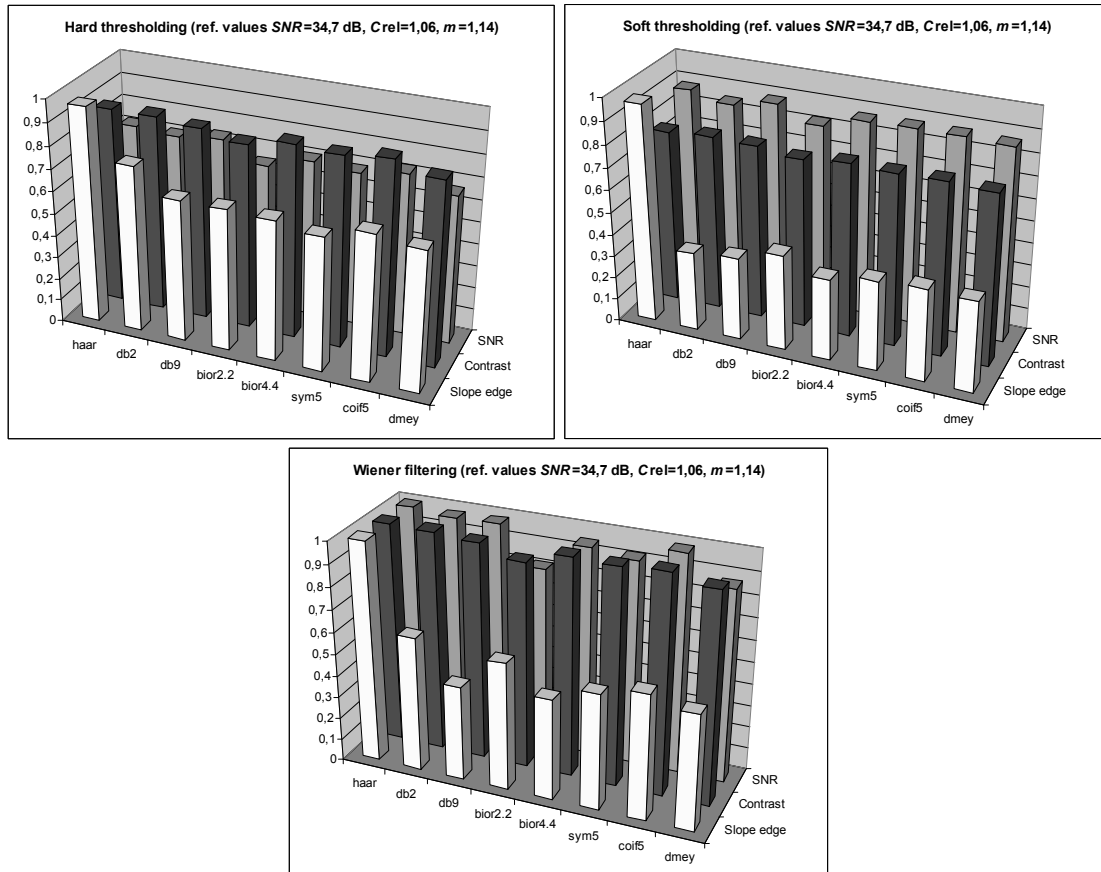


Fig. 5. Results of de-noising of the phantom MR image with SNR = 19.1 dB.

The results of de-noising the phantom MR image with  $SNR = 19.1$  dB are shown in Tab. 2 and Fig. 5. There is a great amount of similarity with previous results excluding the contrast value, where a higher value is achieved for hard thresholding than for soft thresholding because of the better SNR of the original MR image.

While the first tested image (the MR phantom image) does not include almost any detailed information and the image could be evaluated by measuring only one significant edge, in the case of the second tested image (the MR image

of head) the measurement of two various edges was applied, which differed in the magnitude of intensity change in the neighbourhood of the relevant edge (see Fig. 6). The values measured are summarized in Tab. 3, where  $m_1$  defines the linear slope edge approximation with the higher intensity change, and  $m_2$  with the lower intensity change. The resultant graphs can be seen in Fig. 7, but the contrast is not depicted here because of unimportant changes in contrast in individual thresholding techniques and the mother wavelets used.

Wavelet filter	Hard thresholding			Soft thresholding			Wiener filtering		
	$SNR$	$C_{rel}$	$m$	$SNR$	$C_{rel}$	$m$	$SNR$	$C_{rel}$	$m$
haar	25.2	0.93	1.10	30.4	0.95	1.07	34.7	1.06	1.14
db2	24.7	0.93	0.85	29.6	0.96	0.61	34.1	1.05	0.70
db9	25.5	0.91	0.73	30.4	0.95	0.47	34.2	1.03	0.49
bior2.2	22.5	0.87	0.73	28.9	0.95	0.64	28.4	0.98	0.66
bior4.4	24.5	0.91	0.72	29.9	0.95	0.48	32.9	1.04	0.52
sym5	24.0	0.90	0.68	30.1	0.95	0.54	32.1	1.03	0.60
coif5	25.2	0.92	0.75	30.1	0.95	0.56	34.4	1.05	0.65
dmey	23.2	0.87	0.72	30.0	0.95	0.54	30.3	1.01	0.60

Tab. 2. Results of de-noising of the phantom MR image with  $SNR = 19.1$  dB.

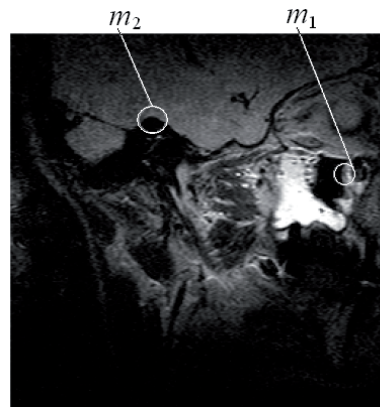


Fig. 6. Test MR image of head with areas of slope edge measurement.

Wavelet filter	Hard thresholding				Soft thresholding				Wiener filtering			
	$SNR$	$C_{rel}$	$m_1$	$m_2$	$SNR$	$C_{rel}$	$m_1$	$m_2$	$SNR$	$C_{rel}$	$m_1$	$m_2$
haar	47.1	0.97	0.99	0.94	50.7	0.97	0.87	0.35	49.8	0.97	0.95	0.79
db2	43.5	0.97	0.97	0.91	47.9	0.97	0.78	0.62	46.9	0.98	0.83	0.72
db9	42.3	0.97	0.98	0.97	49.0	0.97	0.79	0.60	47.4	0.97	0.82	0.86
bior2.2	38.8	0.97	0.98	0.97	46.6	0.97	0.96	0.79	44.4	0.97	1.00	0.91
bior4.4	42.6	0.97	0.97	0.88	49.5	0.97	0.81	0.77	48.4	0.97	0.84	0.87
sym5	43.9	0.97	0.86	0.93	49.8	0.97	0.83	0.59	48.7	0.97	0.86	0.86
coif5	42.7	0.97	0.97	0.73	48.8	0.97	0.80	0.58	47.7	0.97	0.84	0.67
dmey	41.2	0.97	0.98	0.96	48.4	0.97	0.85	0.80	47.1	0.97	0.88	0.90

Tab. 3. Results of de-noising of the MR image of head with  $SNR = 33$  dB.

It can be seen from Fig.7 that the influence of thresholding itself on the resultant MR image of head approximately corresponds to the results for the MR phantom image. Therefore it is possible to say that the choice of threshold method does not depend much on the type of the image being processed. On the other hand, the results of the processed MR images are pretty dependent on the choice of the mother wavelet.

It has been shown that it is advantageous to assign the mother wavelet to the chosen threshold method. The following combinations can be given as examples: hard thresholding and the Haar wavelet, soft thresholding and the bi-orthogonal wavelet 2.2 or the Wiener filtering and

the Coiflet wavelet of the 5<sup>th</sup> order. But the greatest influence on the processing of degraded image can be seen in the choice of the mother wavelet. It is evident both from the differences between the tested images (the Haar wavelet used for the MR phantom image or the bi-orthogonal wavelet 2.2 used for the MR image of head), and even from partial areas of the individual MR images. If we follow the slope ratio of two edges,  $m_1$  and  $m_2$ , for various types of mother wavelet, we suppose that generally the slope edge  $m_2$  is less than  $m_1$ . The ratio is thus high for some types of mother wavelet (the Haar wavelet, for example), but for other wavelets  $m_1$  can be approximately equal to  $m_2$ ;  $m_2$  can even be higher than  $m_1$  (the discrete Meyer wavelet, for example).

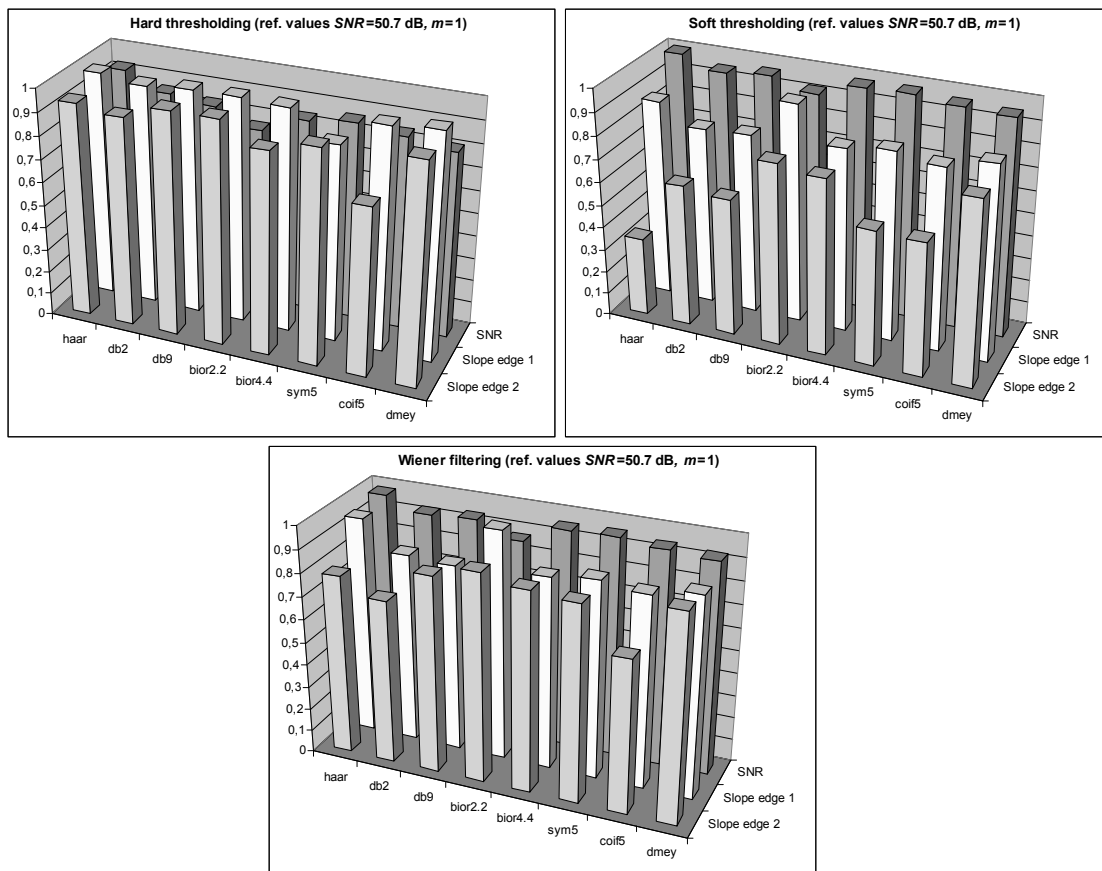


Fig. 7. Results of de-noising of the MR image of head with SNR = 33 dB.

### 4. Conclusion

In this paper, an evaluation of the wavelet-based de-noising efficiency for various mother wavelets is described. The real and imaginary parts of the MR image are filtered separately and the evaluation of filtering efficiency is realized on the output complex MR image, using three parameters: SNR, image intensity contrast, and intensity gradient in chosen parts of the MR image.

Generally speaking, contrast depends on bias, and thus also on the sharpness of the whole image, which is defined by the high slope of edges. Taking in account our experiments, we can claim that this only holds for less

degraded input images. For other input images, the contrast is more dependent on enhancing the SNR than on preserving the steepness of edges.

The effect of the thresholding methods used can be characterized as follows: hard thresholding preserves the edge steepness of the input image and then the resultant contrast is higher. At the same time, SNR is not so high because of discontinuities between cancelled and retained wavelet coefficients. On the other hand, soft thresholding thanks to fewer discontinuities among wavelet coefficients improves the SNR, but reduces the edge steepness (the image is more blurred), and bias is inserted and results in less contrast. The Wiener filtering of the wavelet coeffi-

cients suppresses the disadvantages of the two above-mentioned thresholding methods, but only on condition that parameter  $\tau$  is known apriori. Its value depends on the particular MR image. Therefore, the Wiener filtering is not useful for full automatic processes. It can be said that hard thresholding is useful for high SNR input images, soft thresholding is more convenient for low SNR input images, and, finally, the Wiener filtering is useful for all MR images, but if optimum parameter  $\tau$  can be estimated in advance.

The choice of the mother wavelet (wavelet filter) greatly affects the resultant image quality. Eight various mother wavelets were taken into account in this paper. The Haar wavelet was the most useful for simple images (not many details) with high slope edges (sharp transitions), especially with hard thresholding. The greatest disadvantage of hard thresholding is the difficulty of obtaining smoothly reconstructed images, which shows by disturbing rectangular artifacts. Mother wavelets of the Daubechies type are typical representatives of non-symmetrical wavelets, which are used with both plain images and images with many details (so complicated) to obtain a higher SNR value (but less steep edges, of course). It is the reason why they are combined with soft thresholding. If the order of the Daubechies wavelets increases, then the slope steepness tends to decrease and, on the contrary, SNR becomes higher. Bi-orthogonal wavelets, which belong to symmetrical wavelets, yield a good balance between high slope edge and high SNR for all threshold methods. Consequently, they are optimal wavelets for much complicated images in order to obtain good balance between SNR and image sharpness. Higher-order bi-orthogonal wavelets give outputs similar to wavelets of the Daubechies type. Wavelets of the Coiflet or Symlet type give identical results for plain images. They give a high SNR at the cost of lower slope edge. When the Coiflet and Symlet wavelets were applied to more complicated image, then they differed in edge slope ratios  $m_1$  and  $m_2$  for hard thresholding. It can be said that they behave like the Daubechies wavelets. The discrete Meyer wavelets exhibit advantages that show, in particular, when the Wiener filtering of wavelet coefficients is used for more complex images. A high degree of correspondence between SNR and the preservation of the steepness of the two image edges measured,  $m_1$  and  $m_2$ . A similar correspondence was obtained in the application of soft thresholding. The discrete Meyer wavelet is recommended to be used as a universal mother wavelet for processing complicated images in combination with soft thresholding.

## Acknowledgements

The paper has been supported by the Research Project SIX (CZ.1.05/2.1.00/03.0072), by the Czech Grant Agency under grant No. 102/09/0314 and by the KONTAKT Project ME10123 (Research of Digital Image and Image Sequence Processing Algorithms).

## References

- [1] WEAVER, J. B., XU, Y., HEALY, D. M., CROMWELL, L. D. Filtering noise from images with wavelet transforms. *Magnetic Resonance Medicine*, 1991, vol. 21, p. 288-295.
- [2] HENKELMAN, R. M. Measurement of signal intensity in the presence of noise in MR images. *Medical Physics*, 1985, vol. 12, p. 232-233.
- [3] NOWAK, R. D. Wavelet-based Rician noise removal for magnetic resonance imaging. *IEEE Transactions on Image Processing*, 1999, vol. 8, no. 10, p. 1408-1419.
- [4] ALEXANDER, M. E., BAUMGARTNER, R., SUMMERS, A. R., WINDISCHBERGER, C., KLARHOEFER, M., MOSER, E., SOMORJAI, R. L. A Wavelet-based method for improving signal-to-noise ratio and contrast in MR images. *Magnetic Resonance Imaging*, 2000, vol. 18, p. 169-180.
- [5] ZAROUBI, S., GOELMAN, G. Complex de-noising of MR data via wavelet analysis: Application to functional MRI. *Magnetic Resonance Imaging*, 2000, vol. 18, p. 59-68.
- [6] CRUZ-ENRIQUEZ, H., LORENZO-GIORNI, V. J. Wavelet-based methods for improving signal-to-noise ratio in phase images. *Lecture Notes in Computer Science*, 2005, vol. 3656, p. 247-254.
- [7] ADDISON, P. S. *The Illustrated Wavelet Transform Handbook*. Institute of Physics, 2002.
- [8] VIDAKOVIC, B. *Statistical Modelling by Wavelets (Wiley Series in Probability and Statistics)*. New York: John Wiley&Sons, 1999.
- [9] DONOHO, D. L. De-noising by soft-thresholding. *IEEE Transactions on Information Theory*, vol. 41, 1995.
- [10] BRAUNISH, H., BAEIAN, W., KONG, J., A. Phase unwrapping of SAR interferograms after wavelet ne-noising. *IEEE Geoscience and Remote Sensing Symposium*, 2000, vol. 2, p. 752-754.
- [11] SADASHIVAPP, G., ANANDA BABU, K.V.S. Wavelet filters for image compression, an analytical study. *International Journal on Graphics, Vision and Image Processing*, 2009, vol. 9.
- [12] CANCINO-DE-GREIFF, H. F., RAMOS-GARCIA, R., LORENZO-GIORNI, V. J. Signal de-noising in magnetic resonance spectroscopy using wavelet transforms. *Concepts in Magnetic Resonance*, 2002, vol. 14, p. 388-401.

## About Authors ...

**Karel BARTUSEK** was born in Brno, Czech Republic, in 1948. He received the Ing. (MSc.) degree in Electrical Engineering in 1973, the CSc. (PhD.) degree in 1983, DrSc. degree in 1998 and Prof. degree in 2008. He works as an independent scientific worker at the Institute of Scientific Instruments in Brno, Academy of Sciences of the Czech Republic and as a scientific worker at the Brno University of Technology, Faculty of Electrical Engineering and Communication. He is author/co-author over 200 scientific publications.

**Zdenek SMEKAL** was born in Brno, Czech Republic, in 1949. He received the Ing. (MSc.) degree in Electrical Engineering in 1973, the CSc. (Ph.D.) degree in 1978, and Prof. degree in 2000. He has been involved in international cooperation in the European research project COST - OC G6 10 "Digital Audio Effects" (1997-2001), OC 277

“Nonlinear Signal Processing” (2004-2006) and OC 2102 “Cross-Modal Analysis of Verbal and Nonverbal Communication” (2006-2010). He is interested in basic research of methods of digital signal and image processing in the media-informatics. He is the author of three monographs and more than 200 publications. Since 1998 he is a member of the IEEE (Signal Processing, Communications and Computer Societies), and he obtained the IEEE Senior Member degree in 2006.

**Jiri PRINOSIL** is the academic researcher at the Faculty of Electrical Engineering and Communication, Brno University of Technology. He specializes in the utilizing of digital audio and image signal processing methods into media-informatics. He also deals with proposal of algorithms for biomedical image enhancement and segmentation in cooperation with the medical staff of Masaryk University in Brno. He is author/co-author over 30 scientific publications.